Experimental Thermal and Fluid Science 70 (2016) 270–282

Contents lists available at ScienceDirect

Experimental Thermal and Fluid Science

journal homepage: www.elsevier.com/locate/etfs

Flow pattern transition models and correlations for flow boiling in mini-tubes

Mohamed M. Mahmoud [a,b], Tassos G. Karayiannis [a,*]

[a] School of Engineering and Design, Brunel University London, Uxbridge UB8 3PH, UK
[b] Faculty of Engineering, Zagazig University, Zagazig 44519, Egypt

ARTICLE INFO

Article history:
Received 11 February 2015
Received in revised form 17 September 2015
Accepted 19 September 2015
Available online 26 September 2015

Keywords:
Flow boiling
Mini tubes
Flow patterns
Correlations

ABSTRACT

An evaluation of models and correlations predicting flow patterns in mini-tubes is described in this paper and final recommendations are made for a way forward. Flow boiling patterns of R245fa in a 1.1 mm diameter copper tube were used in this evaluation. The experiments covered an experimental range of mass flux 100–400 kg/m^2 s, heat flux 3–25 kW/m^2, inlet pressure of 1.85 and inlet subcooling of 5 K. Hysteresis was evident in these experiments across the whole range, with obvious changes in the flow patterns between increasing and decreasing heat flux. The four main flow patterns were bubbly, slug, churn and annular flow. Confined flow was also evident. For increasing heat flux, only annular flow was evident but all the flow patterns were evident with decreasing heat flux. Therefore, the evaluation of flow pattern maps carried out in this study was based on the decreasing heat flux data, as this covered the full range of flow patterns. The evaluation of more than ten models and correlations demonstrated that there is no general model that can predict accurately all flow pattern transition boundaries. Only one model succeeded in predicting all transition boundaries very well, except the bubbly to slug transition. Thus, a new modification on this boundary is proposed in this paper that could predict the experimental data used in this study very well.
© 2015 The Authors. Published by Elsevier Inc. This is an open access article under the CC BY license (http://creativecommons.org/licenses/by/4.0/).

1. Introduction

The application of flow boiling in microchannels as a cooling method of high heat flux devices is of great interest to the engineering community. Progress is currently restricted by a limited knowledge of flow patterns and subsequent heat transfer mechanisms and the ability to predict pressure drop and heat transfer rates. A recent review by Mahmoud et al. [1] is available, which includes a section on past work on flow patterns in small to micro diameter tubes. This review demonstrates that: (i) channel size has a significant effect on the morphology of gas–liquid two phase flow, (ii) the most frequently identified flow patterns are bubbly, slug, churn and annular flow with confined bubble flow evident in certain operating ranges, (iii) dispersed bubbly, churn and stratified flow tend to diminish as the diameter decreases. Flow pattern maps and prediction methods are available in literature but these are often restricted to particular experimental conditions and certain fluids. Hassan et al. [2] found large discrepancies in the reported flow patterns in microchannels when previous experimental flow maps were compared against each other. Additionally, they found that channel orientation affects the transition boundaries although many researchers reported insignificant effect. Thus, they proposed two universal maps, one for horizontal and one for vertical channels. The limitation in the development of new accurate flow pattern maps could be attributed to the reasons discussed below.

The first reason is the lack of understanding all the parameters which could affect the flow patterns. Shao et al. [3] thought that the dominating factors for flow pattern transitions are channel size, superficial velocities, liquid phase surface tension and channel wettability. Evaluation of past literature can reveal that there are contradictions among researchers on the effect of these factors. For example, some researchers such as [4–7] agreed on that the transition to annular flow shifts to higher gas superficial velocities as the diameter decreases while researchers [8,9] reported an opposite effect. Some researchers investigated the effect of contact angle (surface wettability) on flow patterns characteristics in macro and microchannels, see for example [10–14]. The definition of contact angle and surface wettability is depicted in Fig. 1. They agreed on that surface wettability has a significant effect on flow patterns. All conventional flow patterns (bubbly, slug, churn, annular) were reported to occur in the highly wetting channels investigated in their study, i.e. θ = 7–45° [10–14]. As contact angle

* Corresponding author.
E-mail address: tassos.karayiannis@brunel.ac.uk (T.G. Karayiannis).

http://dx.doi.org/10.1016/j.expthermflusci.2015.09.023
0894-1777/© 2015 The Authors. Published by Elsevier Inc.
This is an open access article under the CC BY license (http://creativecommons.org/licenses/by/4.0/).

Nomenclature

Bd	bond number (–), $g\Delta\rho D^2/\sigma$
Bo	boiling number (–), q/Gh_{fg}
C_0	distribution parameter
Ca	capillary number (–), $Ca = \mu u/\sigma$
Co	confinement number (–), $\frac{1}{D}\sqrt{\sigma/g\Delta\rho}$
c_1	experimental coefficient for critical void fraction on bubbly slug boundary, Eq. (16)
c_2	experimental exponent for critical void fraction on bubbly-slug boundary, Eq. (16)
D	tube diameter (m)
D_b	bubble diameter (m)
d_c	critical bubble diameter, Eq. (21) (m)
$d_{\max}$	maximum bubble diameter (m)
$(d_{\max})_0$	maximum bubble diameter for dilute dispersion (m)
$(d_{\max})_\alpha$	maximum bubble diameter for denes dispersion (m)
Eo	Eotvos number (–), $g\Delta\rho D^2/8\sigma$
Fr_{gs}	Froude number based on gas superficial velocity, $Fr_{gs} = u_{gs}/\sqrt{gD}$
Fr^*_{gs}	modified Froude number based on gas superficial velocity, $Fr^*_{gs} = u_{gs}\sqrt{\rho_g/(\rho_l-\rho_g)gD}$
f_l	friction factor based on homogeneous velocity
g	gravitational acceleration (m/s^2)
G	mass flux (kg/m^2 s)
k	Constant in Eq. (5)
K	Constant in Eq. (20)
P	pressure (Pa)
P_g	gas pressure (Pa)
P_l	liquid pressure (Pa)
q	heat flux (W/m^2)
Re_{go}	Reynolds number based on all flow as gas, $\mathrm{Re}_{go} = GD/\mu_g$
Re_{gs}	Reynolds number based on gas superficial velocity, $\mathrm{Re}_{gs} = \rho_g u_{gs} D/\mu_g$
Re_h	Reynolds number based on homogeneous velocity, $\mathrm{Re}_h = \rho_l u_h D/\mu_l$
Re_{lo}	Reynolds number based on all flow as liquid, $\mathrm{Re}_{lo} = GD/\mu_l$
Re_{ls}	Reynolds number based on liquid superficial velocity, $\mathrm{Re}_{ls} = \rho_l u_{ls} D/\mu_l$
Su	Suratman number, $Su = \mathrm{Re}_{ls}/Ca_{ls}$
T_{sat}	Saturation temperature (°C)
u_d	drift velocity (m/s)
u_{gs}	gas superficial velocity (m/s)
u_h	homogeneous velocity (m/s), $u_h = u_{gs} + u_{ls}$
u_l	liquid velocity defined by Eq. (20)
u_{ls}	liquid superficial velocity (m/s)
U_g	actual gas velocity (m/s)
U_l	actual liquid velocity (m/s)
U_r	relative velocity, $(U_g - U_l)$
We_b	Weber number based on bubble diameter and homogeneous velocity, $We_b = \rho_g u_h^2 d_c/\sigma$
We_{gs}	Weber number based on gas superficial velocity, $We_{gs} = \rho_g u_{gs}^2 D/\sigma$
We_{ls}	Weber number based on liquid superficial velocity, $We_{ls} = \rho_l u_{ls}^2 D/\sigma$
We_g	gas Weber number based on total mass flux, $We_g = G^2 D/\rho_g\sigma$
We_l	liquid Weber number based on total mass flux, $We_l = G^2 D/\rho_l\sigma$
We_r	liquid Weber number based on the relative actual velocity, Eq. (38)
x	horizontal axis (–)
x_e	exit vapor quality (–)
$x_{IB/CB}$	vapor quality at the transition from isolated bubble to coalescing bubble regime
$x_{CB/A}$	vapor quality at the transition from coalescing bubble to annular regime
y	vertical axis (–)

Greek symbols

α	void fraction
α_{act}	actual void fraction
α_{cal}	calculated void fraction, $u_{gs}/(u_{gs}+u_{ls})$
α_c	critical void fraction
θ	contact angle (°)
μ_g	gas dynamic viscosity (kg/m s)
μ_l	liquid dynamic viscosity (kg/m s)
ρ_g	gas density (kg/m^3)
ρ_l	liquid density (kg/m^3)
σ	surface tension (N/m)

increases (low wettability), the liquid film around the slug becomes thicker and unstable resulting in a new pattern called rivulet flow, which replaces churn flow. On the contrary, Wang et al. [15] reported that reducing surface wettability (increasing θ) did not induce the appearance of new flow patterns. They reported slug, slug-annular, annular and parallel flow (stratified) within a contact angle range θ = 37–135°.

Another example of contradiction found in the literature, is the effect of surface tension. Some researchers such as [6,7,15–17] agreed that the transition lines shift to lower gas superficial velocities as surface tension decreases. On the contrary, researchers [18,19] reported an opposite effect. Moreover, the contradiction on the relative importance of the above factors, i.e. wettability and surface tension, can also be detected from the various coordinates used for plotting the flow maps. For example, researchers [2,16,20] plotted their maps as a function of the superficial liquid and gas velocities. This means that the effect of other parameters such as wettability, surface tension, viscosity, density is not included. Other researchers such as [6,21] plotted their maps as a function of liquid and gas Weber numbers, which consider the effect of diameter, velocity, density and surface tension.

The second reason is the fact that developing accurate flow maps and transition models requires a large databank of results with varying fluid properties, channel size and experimental conditions. This is currently hindered by the discrepancies found in the available data as discussed above, even when using the same refrigerant and channel diameter. Karayiannis et al. [22] suggested that these discrepancies were due to the surface characteristics and heated length. As indicated by Consolini et al. [23], flow stability was also an important factor. A study by Mahmoud et al. [24] into the effects of surface characteristics using seamless and

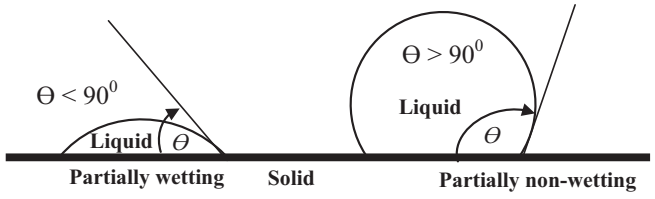

Fig. 1. Definition of surface wettability and contact angle (θ).

welded stainless steel tubes found a difference in the heat flux value at the occurrence of the first bubbles (with the welded tube requiring a higher heat flux) and the trend in the heat transfer coefficient with quality or distance along the tube. The inner surface of these tubes was analyzed using Scanning Electron Microscope (SEM). The results demonstrated that the surface of the welded tube was very smooth with some local damages while that of the cold drawn tube has random scratches or channels uniformly distributed along the tube, which could act as a nucleation cavity. However, in the study of [24], the flow patterns for both tubes were similar.

The third reason is the contradiction in the method of defining the flow patterns. There are variances in both the flow patterns seen and the terminology used to define the flow patterns. Also, distinguishing and classifying the main regime into various sub-regimes is a common difference. For example, Chen et al. [6] distinguished between bubbly and dispersed bubbly flow, while Mishima and Ishii [20] did not. Coleman and Garimella [25] classified annular flow into five sub-regimes namely; annular mist, annular ring, wavy ring, wave packet and annular film. On the contrary, Thome et al. [26] recommend that the primary flow regimes (bubbly, slug, annular and mist flows) should be unified and standardized in order to avoid the variance in terminology for the same flow regime. Also, they recommended the development of multi-scale maps in order to have more details about each flow pattern. Baldassari and Marengo [27] attributed the discrepancies in flow patterns reported to the difficulty in identifying flow patterns using objective methods and the increasing errors with decreasing diameter.

The fourth reason is the fact that no consideration is usually given to (i) surface finish, (ii) channel material and (iii) hysteresis. The present authors believe that these factors are very important at micro scale. However, very limited past research papers exist covering the effect of these parameters on flow patterns. Kubiak et al. [28] reported that surface roughness and material have a significant effect on surface wettability (contact angle). They investigated experimentally the effect of surface roughness on the apparent contact angle using a wide range of materials including aluminum alloy, titanium alloy, steel alloy, copper alloy, ceramic and poly-methylmethacrylate (PMMA). For all tested materials, the contact angle decreased to a minimum value then increased again with increasing surface roughness. This complex behavior of contact angle with roughness may result in a complex effect on flow boiling heat transfer and flow patterns. This is due to the fact that, practically, surface roughness is not uniformly distributed along the test tubes. Accordingly, nucleation characteristics are also expected to be affected. This may result in a large variance in bubble generation frequency which might affect the flow pattern transition mechanisms. Based on measuring the bubble frequency, Revellin and Thome [9] classified the flow regimes into: (i) isolated bubble regime in which the bubble generation frequency increases with heat flux up to a maximum value, (ii) coalescing bubble regime in which the frequency is decreasing with heat flux due to bubble coalescence, (iii) annular flow regime in which the frequency becomes zero. In adiabatic gas–liquid flow in microchannels, the inlet conditions can have a significant effect on the resulting flow patterns [29–31]. In a similar manner, in diabatic flows, the different surface finish characteristics of the microchannel can affect the prevailing flow patterns.

It is obvious from the above review that no experimental study considered hysteresis in flow boiling patterns. Only one study by Barajas and Panton [10] for adiabatic gas–liquid flow in a 1.6 mm tube reported some hysteresis on the slug-annular transition boundary when the experiments were conducted in the opposite direction (decreasing gas flow rate). The R245fa data in a 1.1 mm diameter vertical tube used in this study were obtained from experiments with decreasing heat flux, see Pike-Wilson [32] and Karayiannis et al. [33]. These data were used to assess existing flow pattern maps and transition models in order to have an insight on the transition mechanisms. Recommendations subsequently are for the prediction of flow patterns transition boundaries.

2. Experimental methodology used in obtaining the data

The data used in the present study were obtained from experiments carried out over a range of heat and mass fluxes, i.e. 3–25 kW/m^2 and 100–400 kg/m^2 s, for inlet pressure of 1.85 bar using R245fa in a 1.1 mm diameter tube, see Refs. [32,33]. The tube was made of copper and the flow was vertically upward. The test facility was previously used to investigate heat transfer and flow patterns of R134a in small to micro diameter tubes. Details of this and the test facility can be found in Huo et al. [34], Mahmoud et al. [1] and Pike-Wilson and Karayiannis [35]. The test section consisted of a pre-heater to control the inlet temperature followed by a 150 mm adiabatic calming section, to ensure fully developed flow. The copper test section was 300 mm long and heated directly using DC current with the supplied power being measured using a Yokogawa power meter WT110 with a manufacturer recorded accuracy of ±0.29%. The inlet and outlet temperatures were measured using T-type thermocouples with an accuracy of ±0.18 K. Pressure transducers were used at these locations to record the pressure with an accuracy of ±1.5%. The pressure drop across the heated section was measured with a differential pressure transducer (PX771A-025DI) with an accuracy of ±0.08%. Fourteen equidistant K-type thermocouples were attached to the heated section using electrically insulating and thermally conducting epoxy, with a mean absolute error of ±0.23 K. Heat transfer and pressure drop data were recorded over a 90 s period, simultaneously as flow pattern data being recorded. Flow visualization was possible through a borosilicate glass tube, of 1.1 mm internal diameter, which was located at the heated section outlet. The high speed camera (Photo-Sonics Phantom V4B/W) recorded at 1000 frames per second with a resolution of 512 × 512 pixels. Data were recorded when the test facility was deemed to be in a steady state based on oscillations in the mass flow rate, pressure and temperatures at the inlet, see Karayiannis et al. [22].

3. Results and discussion

The flow patterns in small to micro diameter tubes are commonly defined as bubbly, confined bubble, slug, churn and annular flow. Note that in the work of Chen et al. [6] for R134a, in stainless steel tubes with diameters ranging from 1.1 mm to 4.26 mm, very clear photographs of dispersed bubble flow were observed. In this regime, the bubbles were more in number and much smaller than what were referred to in Chen et al. and here in this paper as bubbly flow. In the data used in [32,33], the flow patterns for an increasing heat flux were limited to some occurrence of slug and churn flow and a dominance of annular flow. This result agrees with the results of Consolini and Thome [23] for flow boiling of R245fa in a 0.5 mm diameter stainless steel tube. They did not see bubbly and slug flows and churn and annular flows were the dominant regimes. It is interesting to note that earlier Revellin and Thome [9] conducted the same test using R245fa, with the same experimental facility, tube material and diameter. They observed all flow patterns; bubbly, bubbly/slug, slug, semi-annular and annular flows. The difference between the two results could be attributed to testing two tubes with different surface finish. It was proved that commercially available tubes do not have uniform surface finish along the length of the tube, see Karayiannis et al. [22]. In the study of [32,33], all the commonly observed flow

patterns (bubbly, confined bubble, slug, churn and annular flow) were observed only with decreasing heat flux. Therefore, the comparison with flow pattern maps presented in the next section is based on the decreasing heat flux results of [32,33]. The difference in flow patterns seen for increasing and decreasing heat fluxes was thought to be as a result of hysteresis. Nucleation site activation is related to the wall superheat, with smaller cavities requiring a larger wall superheat to be activated. The wall superheat is higher with increasing heat flux than for decreasing heat flux. This higher wall superheat should allow for small nucleation sites to be activated with increasing heat flux. These can remain active when the heat flux is then decreased, resulting in flow patterns which were not seen for increasing heat flux. For all mass fluxes, annular flow was the dominant flow pattern [32,33]. Fig. 2 presents the flow patterns at a mass flux of 200 kg/m^2 s. Pike-Wilson and Karayiannis [35] reported experiments with tubes made of three materials, namely stainless steel, brass and copper (the latter is used for the data of this paper), all with a diameter of 1.1 mm. The flow patterns of Fig. 2 were evident for all three tubes with a decreasing heat flux but at different exit qualities and heat fluxes, which indicates some effect of surface characteristics.

4. Flow pattern maps

This section presents a detailed comparison with existing flow pattern maps and transition models developed for micro scale applications under adiabatic and diabatic conditions. The experimental data of [32,33] used for comparison are also compared with experimental data of some researchers who reported similar flow patterns even if the diameter was smaller than 1 mm. Additionally, the comparison includes some flow pattern maps developed for large diameter channels at microgravity due to the similarity with microchannels as reported by Akbar et al. [21]. As previously mentioned, the flow pattern data used in this study were for inlet pressure of 1.85 bar. Each model is reviewed very briefly in order to understand the differences between existing models and the mechanisms based on which the transition criteria were proposed.

5. Comparison with Rezkallah [36]

Based on the relative importance of surface tension and inertia forces, Rezkallah and co-workers classified flow patterns into the following: (1) surface tension dominated region, which includes bubbly and slug flow, (2) inertia dominated region which includes annular flow, (3) transition region in which surface tension and inertia forces are comparable and includes slug-annular/churn flow. In a previous work by Rezkallah and co-workers [37,38] the transition from one region to the other was proposed to occur at constant gas Weber number: $We_{gs} \leqslant 1$ for surface tension dominated region and $We_{gs} \geqslant 20$ for the inertia dominated region. Rezkallah [36] reassessed these criteria using a large experimental databank from literature and found that $We_{gs} \propto We_{ls}^{0.25}$ at transition, i.e. there is some dependency on gas superficial velocity. Fig. 3 depicts the comparison of the experimental data of [32,33] with the modified version of the map on a $u_{ls} - u_{gs}$ plane. It is shown that there is a reasonable prediction for bubbly, slug and churn flows while there is a poor prediction for annular flow. The annular flow data, which were deemed to be inertia dominated, are located inside the transition region. This transition criterion predicts annular flow to occur at very high superficial gas velocities compared to the experimental data. Also, this map predicts bubbly and slug flow to exist at very low gas and liquid superficial velocities. It is noteworthy that the slope of the lines is almost similar to the experimental slope. These criteria ($We_{gs} \propto We_{ls}^{0.25}$) were written in the form of Eq. (1) below which demonstrates that the transitional gas velocity depends on liquid to gas density ratio, surface tension, gas density and channel diameter. As the diameter increases, transition occurs early at lower gas velocity (the lines shift to the left) while increasing surface tension and density ratio show an opposite effect.

$$u_{gs} \propto (\sigma/\rho_g D)^{0.375} (\rho_l/\rho_g)^{0.125} u_{ls}^{0.25} \tag{1}$$

6. Comparison with Jayawardena and Balakotaiah [39]

Three dimensionless groups were deemed to be important by Jayawardena and Balakotaiah [39]. These include the liquid and gas Reynolds number and Suratman number Su ($Su = \mathrm{Re}_{ls}/Ca_{ls} = \rho_l D\sigma/\mu_l^2$). All Reynolds numbers were defined based on superficial velocities, see nomenclature. The data were plotted in the form of Su versus $\mathrm{Re}_{gs}/\mathrm{Re}_{ls}$ and fitted to give the transition criteria: Eq. (2) for bubbly to slug and Eq. (3) for slug to annular flow.

$$\left(\frac{\mathrm{Re}_{gs}}{\mathrm{Re}_{ls}}\right) = 464.16 Su^{-2/3}, \quad 10^4 < Su < 10^7 \tag{2}$$

$$\left(\frac{\mathrm{Re}_{gs}}{\mathrm{Re}_{ls}}\right) = 4641.6 Su^{-2/3}, \quad Su < 10^6$$
$$\mathrm{Re}_{gs} = 2 \times 10^{-9}\, Su^2, \quad Su > 10^6 \tag{3}$$

The experimental data used in the present study satisfies the first condition in Eq. (3), i.e. $Su < 10^6$. Fig. 4 shows the comparison with these criteria on $u_{ls} - u_{gs}$ plane. It is obvious that these criteria predict transition to occur at much lower gas superficial velocities

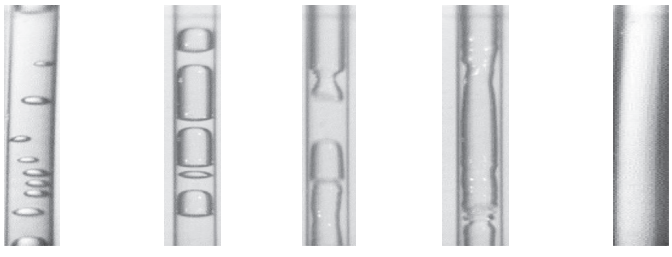

Bubbly	Confined	Slug	Churn	Annular
x_e= 0.008	x_e= 0.017	x_e= 0.054	x_e= 0.099	x_e= 0.14
q=1.1	q=2.0	q=3.3	q=4.6	q=6.7 kW/m^2

Fig. 2. Flow patterns at G = 200 kg/m^2 s and P = 1.85 bar with a decreasing heat flux [32,33].

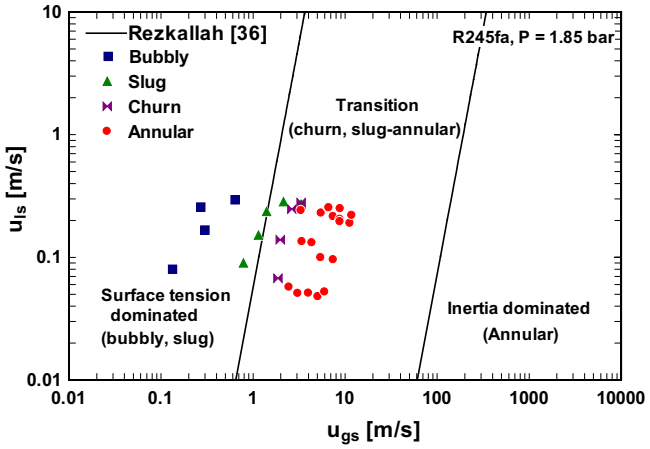

Fig. 3. Comparison of experimental data [32,33] with Rezkallah [36].

compared to the experimental data. The slope of the transition line between bubbly and slug flow is the same as the experimental data. Bubbly flow was predicted to occur at liquid superficial velocities greater than about 0.02 m/s. However, the transition line between slug and annular flow exhibits strong dependency on gas superficial velocity, which is not the case for the experimental data. Writing Eqs. (2) or (3) (by the present authors) in dimensional form results in Eq. (4) below, which shows that the gas superficial velocity at transition decreases with increasing diameter and surface tension but increases with density ratio and viscosity ratio. The effect of surface tension contradicts Eq. (1) given by Rezkallah [36] which states that gas superficial velocity increases with surface tension.

$$u_{gs} \propto (\rho_l \sigma D/\mu_l^2)^{-2/3}(\rho_l/\rho_g)(\mu_g/\mu_l)u_{ls} \tag{4}$$

7. Comparison with Zhao and Hu [40] slug/annular transition model

This model was proposed also for microgravity applications. It was based on the assumption that transition from slug to annular flow occurs when the impulsive force due to gas inertia is sufficient to overcome surface tension force. Instead of defining the impulsive force based on the actual gas velocity as was proposed by previous researchers, they used the actual relative velocity $(U_g - U_l)$. Since transition occurred from slug to annular (no churn), the void fraction from the drift flux model with zero drift velocity and 1.16 for the distribution parameter C_0 was proposed to calculate the superficial velocities. Accordingly, the final expression for the transition criterion is given by Eq. (5) below.

$$\frac{\rho_g u_{gs}(U_g - U_l)D\alpha^{0.5}}{4\sigma} = k \tag{5}$$

The constant k in Eq. (5) was determined empirically and the value was found to be 0.8. Fig. 5 depicts the comparison with this model and shows good agreement with the experimental data. The model predicts annular flow to occur at slightly lower gas superficial velocity compared to the experimental data, particularly as mass flux increases. The only properties included in this equation are gas density and surface tension. The good agreement with the experimental data could be due to the fact that the conventional churn flow with large chaotic nature was not observed in the experimental data described in [32,33]. What is called churn flow herein this study resulted from merging elongated slugs, see Fig. 2. This is matching the assumed transition mechanism by Zhao and Hu [40]. This criterion indicates that as surface tension increases the transition line shifts to the right to occur at higher gas superficial velocity.

8. Comparison with Akbar et al. [21]

This map was developed based on available experimental data in literature for air–water flow in channels with diameter ranging from 0.87 to 1.6 mm. The map was divided into four regions: surface tension dominated region (bubbly, slug, plug), inertia dominated region I (annular, wavy annular), inertia dominated region II (dispersed flow), and transition region. Plotting all data on the Weber number coordinate map, Akbar et al. correlated the data into three transition criteria. These criteria are given by Eq. (6) for the surface tension dominated zone, Eq. (7) for the inertia dominated zone I (annular flow), and Eq. (8) for the inertia dominated zone II (dispersion regime).

$$\begin{aligned} We_{gs} &\leqslant 0.11 We_{ls}^{0.315} \quad \text{for} \quad We_{ls} \leqslant 3 \\ We_{gs} &\leqslant 1, \quad \text{for} \quad We_{ls} > 3 \end{aligned} \tag{6}$$

$$We_{gs} \geqslant 11 We_{ls}^{0.14}, \quad \text{for} \quad We_{ls} \leqslant 3 \tag{7}$$

$$We_{gs} > 1, \quad \text{for} \quad We_{ls} > 3 \tag{8}$$

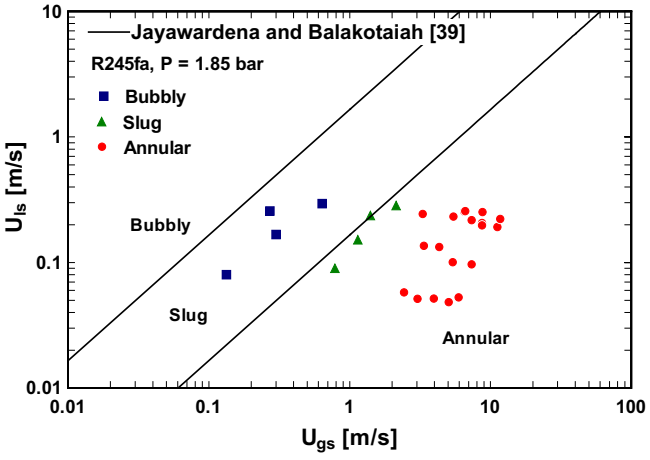

Fig. 4. Comparison of experimental data [32,33] with Jayawardena and Balakotaiah [39].

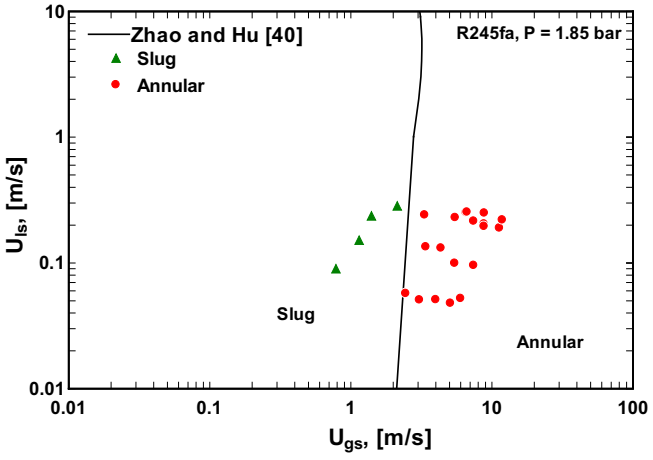

Fig. 5. Comparison of experimental data [32,33] with Zhao and Hu [40].

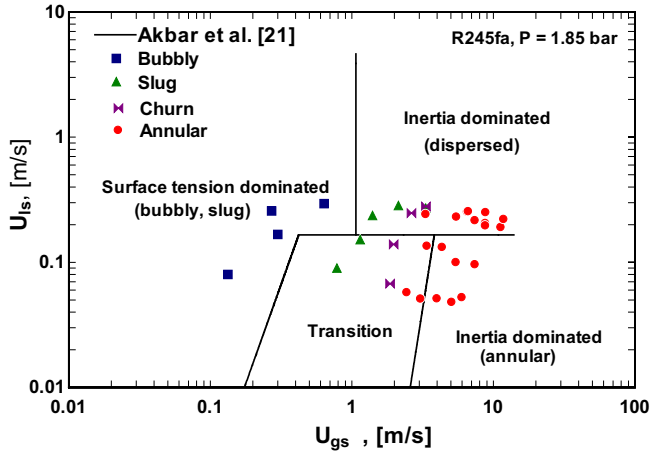

Fig. 6. Comparison of experimental data [32,33] with Akbar et al. [21].

Fig. 6 depicts the comparison with this empirical flow pattern map. It is clear that the map predicts bubbly flow well where the data points are located in the surface tension dominated zone. Slug flow is poorly predicted. For churn and annular flow, the map works better at low liquid superficial velocity. As liquid superficial velocity increases the map exhibits poor predictions where some of the data are located inside the dispersed flow region. Additionally, the map indicates that the transition region occupies a considerable area on the map although this region is expected to be narrower in microchannels. In addition to that, bubbly and slug flows are also predicted to occur at very low gas and liquid superficial velocities.

9. Comparison with Hassan et al. [2]

This map was developed based on 1475 data points collected from the literature and their experimental data using air–water and tubes of diameter 0.8 and 1 mm. Four main regimes were defined to develop the map: bubbly, intermittent, churn and annular flow. Fig. 7 presents a comparison of the experimental data [32,33] with the predictions of the vertical flow pattern map of Hassan et al. [2] based on superficial velocities. In Hassan et al. the intermittent region includes plug and slug flow. This map covers a larger range of superficial gas and liquid velocities than seen with the experimental data used in this paper. The annular flow transition is predicted moderately well. The bubbly and slug flow are predicted to occur at a lower superficial gas velocity than seen experimentally. Additionally, the map predicts that bubbly flow exists only after a certain liquid superficial velocity (u_{ls} > 0.06 m/s) not like the maps of Rezkallah [36] and Akbar et al. [21] where the transition line intersects with the vertical axis (liquid superficial velocity) at negative values.

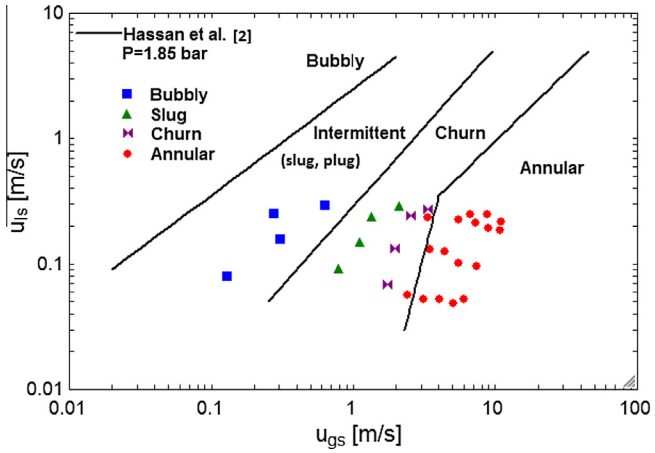

Fig. 7. Comparison of experimental data [32,33] with Hassan et al. [2].

10. Comparison with Chen [33,41]

Chen developed detailed maps based on the liquid and vapor superficial velocities and gave transition criteria using dimensional and dimensionless groups. These criteria were based on 2392 experimental data points covering upward flow boiling of R134a, inlet pressures 6, 10 and 14 bar and corresponding vapor quality and mass flux ranges of 0.05–90% and 50–6400 kg/m^2 s. Fig. 8 depicts the proposed map plotted by Chen [33,41] for 2.01 mm tube at 10 bar as an example just to help in explaining the model. Chen used the same experimental facility as the one used in [32,33] and stainless steel tubes of diameters 4.26, 2.88, 2.01 and 1.1 mm. The flow patterns were viewed at the same location as described in [32,33], through the borosilicate glass tube located at the exit of the heated test section. Chen gave the following equations that describe the transition lines of the flow map shown in Fig. 8:

Churn-annular transition boundary: this boundary was obtained by fitting the experimental data into the form given by Eq. (9) for line A and Eq. (10) for line B, see Fig. 8.

$$We_{ls} = 1.567 \times 10^{-17} (Fr_{gs}\mathrm{Re}_{gs})^{3.41} \tag{9}$$

$$Fr_{gs}\mathrm{Re}_{gs} = 3.119 \times 10^{5} \tag{10}$$

Slug-churn transition boundary: this boundary was described using three equations namely, Eq. (11) for line G, Eq. (12) for line H and Eq. (13) for line I as given below and shown in Fig. 8. Again, these equations were obtained by fitting the experimental data produced by Chen [41].

$$\mathrm{Re}_{ls} = 81.08 We_{gs}^{1.626} Fr_{gs}^{*-0.267} \tag{11}$$

$$u_{gs} = 587.1 \left(\frac{\mu_l}{\rho_g D}\right)^{1.447} \left(\frac{\rho_g D}{\sigma}\right)^{0.937} \tag{12}$$

$$u_h = 2.75 \sqrt{\frac{\sigma}{f_l \rho_l D}} \tag{13}$$

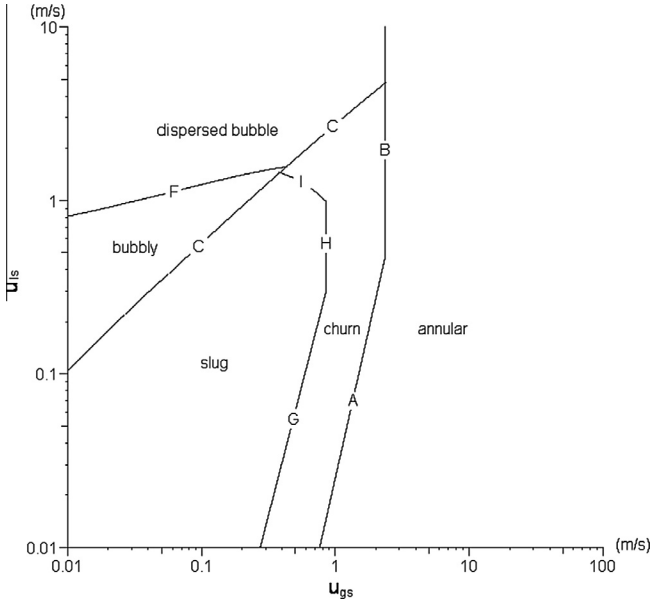

Fig. 8. Flow pattern transition boundaries defined in Chen [41] and reported in Karayiannis et al. [33] for D = 2.01 mm and P = 10 bar.

Chen stated that this transition boundary occurs due to three different mechanisms. The first is bubble elongation which occurs at low liquid superficial velocity (line G). At a certain bubble length the bubble starts to distort. The second is the deformation of the slug nose and tail due to the presence of chaotic flow field in the tail region at an intermediate liquid superficial velocity range (line H). The third mechanism occurs at high liquid superficial velocity (line I) where the bubble cannot keep its regular shape due to the dominance of turbulence over surface tension force. Accordingly, the fanning friction factor f_l in Eq. (13) is calculated based on turbulent flow and the homogeneous Reynolds number as given by Eq. (14) below which is cited in Jayanti and Hewitt [42].

$$f_l = 0.046\mathrm{Re}_h^{-0.2} \tag{14}$$

Bubbly-slug and dispersed bubble-churn transition boundaries: this boundary (line C in Fig. 8) was proposed to occur when the void fraction α in Eq. (15) below equals a critical value (α_c). Some researchers found that the void fraction at which bubbly-slug and dispersed bubble-churn transition occurs does not depend on experimental conditions. For example, Taitel [43] found that the critical void fraction value is 0.25 for bubbly-slug transition and 0.52 for dispersed bubble-churn transition. Contrary to that, Chen found that the critical void fraction depends on experimental conditions (diameter, pressure, fluid properties). As a result, he gave a correlation for the critical void fraction, see Eq. (16).

$$u_{ls} = \left(\frac{1}{\alpha C_0} - 1\right) u_{gs} - \frac{u_d}{C_0} \tag{15}$$

$$\alpha_c = c_1 (u_{gs} + u_{ls})^{c_2} \tag{16}$$

Chen plotted the void fraction at which transition occurs (α_c) versus the homogeneous velocity ($u_{gs} + u_{ls}$) and fitted the data to get c_1 and c_2. The values of these constants were found to be $c_1 = 0.138$ and $c_2 = 0.344$. Chen did not propose a correlation for the distribution parameter and the drift velocity in Eq. (15). Instead, he used measured values which depend on pressure and diameter. Thus, Eqs. (17) and (18) cited in Mishima and Ishii [44] were recommended by Karayiannis et al. [33] to generalize this model. It is worth mentioning that Eq. (16) is valid for both dispersed bubble-churn and bubbly-slug transition boundaries as reported by Chen.

$$C_0 = 1.2 - 0.2\sqrt{\rho_g/\rho_l} \tag{17}$$

$$u_d = 0.35\sqrt{gD(\rho_l - \rho_g)/\rho_l} \tag{18}$$

Dispersed bubble-bubbly transition boundary: this boundary (line F in Fig. 8) is given by Eq. (19) and is not included in the present comparison, i.e. no dispersed flow was reported in [32,33].

$$u_l = 0.45\left[1 + 4\left(\alpha_{act}\mathrm{We}_b^{1/2}\right)^{1/3}\right]\left(\frac{\sigma}{f_l \rho_l d_c}\right)^{1/2} \tag{19}$$

Since the actual void fraction (α_{act}) for R134a was found to be less than the calculated one ($\alpha_{cal} = u_{gs}/(u_{gs} + u_{ls})$), a correction factor K such that $\alpha_{act} = K\alpha_{cal}$ was recommended by Chen [41]. As a result, the liquid velocity u_l was given by Eq. (20) below and the values of K are summarized in Table 1 for D = 1.1–4.26 mm and P = 6–14 bar.

$$u_l = \frac{(\rho_g u_{gs} + \rho_l u_{ls})(u_{gs} + u_{ls})}{K(\rho_g u_{gs} - \rho_l u_{gs}) + \rho_l (u_{gs} + u_{ls})} \tag{20}$$

Again, due to the fact that this transition boundary occurs at high liquid velocity, the turbulent condition is dominating. Therefore, f_l in Eq. (19) is calculated as discussed above using Eq. (14). The critical bubble diameter d_c is given by Barnea et al. [45] and defined by Eq. (21) below.

Table 1
The correction coefficient K for the void fraction for R134a given by Chen [41] and cited in Karayiannis et al. [33].

D = 1.1 mm			
P [bar]	6	10	14
K	0.212	0.24	0.296
D = 2.01 mm			
P [bar]	6	10	14
K	0.4	0.604	0.625
D = 2.88 mm			
P [bar]	6	10	14
K	0.181	0.371	0.624
D = 4.26 mm			
P [bar]	6	10	14
K	0.299	0.391	0.562

$$d_c = 2\left[\frac{0.4\sigma}{(\rho_l - \rho_g)g}\right]^{1/2} \tag{21}$$

The general applicability of Eq. (19) for flow boiling needs to be considered further since the K factors proposed are based on R134a data only.

Fig. 9 compares the transition boundaries calculated from the equations above (obtained from R134a data) with the data used in the present study for R245fa [32,33]. Note that Eq. (19) is not included as dispersed flow was not observed for R245fa in the experimental conditions and data used in this paper. This flow pattern map showed much better predictions compared to the maps discussed above. The slug, churn and annular flow patterns are predicted very well. On the contrary, the bubbly-slug transition boundary exhibited high deviation compared to the experimental values, where bubbly flow is predicted to occur at a much higher liquid superficial velocities. This may be attributed to the fact that bubbly flow in the current study occurred only due to nucleation site hysteresis when the heat flux was decreased, which was not the case in the study of Chen [41]. This hysteresis could be the result of surface characteristics (copper in the data used in the present study versus stainless steel in the Chen [41] study). A comparison of Figs. 7 and 9 shows a similarity in the predicted annular transition at lower superficial liquid velocities. Also, it is worth noting that, the predicted transition for bubbly flow shows a similar gradient and deviation as the prediction by Hassan et al. [2]. It is interesting to note that, the slug-churn and churn-annular transition lines shift to the right as the diameter decreases, i.e. transition occurs at higher gas superficial velocities. The effect

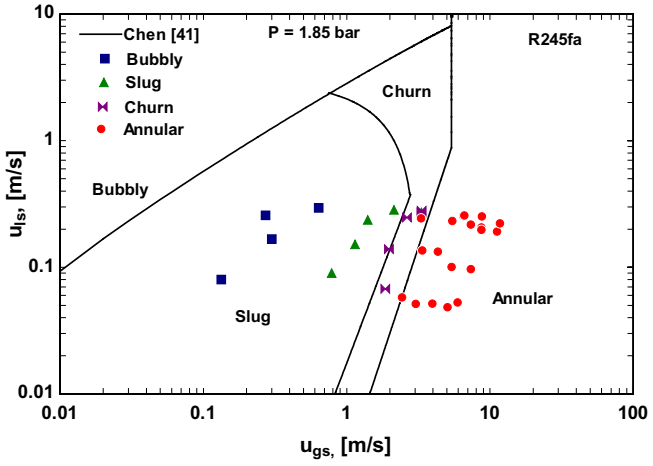

Fig. 9. Comparison of experimental data [32,33] with the predictions of the equations given in Chen [41] and Karayiannis et al. [33].

of diameter on slug-churn boundary is greater than the effect on the churn-annular. In other words, as the diameter decreases, the slug area becomes larger while the churn area tends to diminish, which is a feature of microchannels. Additionally, as surface tension increases these boundaries shift to higher gas superficial velocity.

As previously mentioned, Chen [41] reported three different mechanisms for the transition from slug to churn, see Eqs. (11)–(13) which are corresponding to lines *G*, *H* and *I* in Fig. 8. Inspecting Fig. 9, one can see that the slug-churn transition boundary is only represented by lines *G* and *I* while line *H* is not included which needs a comment. According to Fig. 8 for R134a, line *I* intersects with line *H* at high liquid superficial velocity, which is greater than that at the intersection of line *G* with line *H*. On the contrary, for R245fa, line *I* was found to intersect with line *H* at very low liquid superficial velocity which crosses the annular region. This means that the slug-churn mechanism corresponding to line *H* (disturbance at the tail of the slugs) seems to diminish for this fluid. Fig. 2 may support this point where no chaotic disturbance at the tail of the slugs was observed. In other words, the other two mechanisms (line *G* and *I*) are dominating. Inspecting Eqs. (11)–(13) one can see that these mechanisms depend on fluid properties. This transition boundary needs to be studied further due to the effect of fluid on the most dominant transition mechanism.

11. Comparison with Revellin and Thome [46], Ong and Thome [19] and Costa-Patry et al. [47]

Revellin and Thome [46] proposed a map based on measuring the bubble generation frequency using an optical technique. Their database covered fluids R134a, R245fa, $D = 0.509$, 0.79 mm, $G = 200$–2000 kg/m^2 s, $T_{sat} = 26$–35 °C and heat flux up to 597 kW/m^2, inlet sub-cooling 2–15 K and evaporator length 20–70 mm. The visualization was conducted in a glass tube located at the exit of the evaporator. The flow patterns were classified into the following: (1) isolated bubble regime (IB), which included bubbly and/or slug flows, (2) coalescing bubble regime (CB), and (3) annular regime (A). The proposed transition criteria are given by Eq. (22) for the transition from IB to CB and Eq. (23) for the transition from IB to A.

$$x_{IB/CB} = 0.763\left(\frac{\mathrm{Re}_{lo}Bo}{We_g}\right)^{0.41} \tag{22}$$

$$x_{CB/A} = 0.00014\mathrm{Re}_{lo}^{1.47}We_l^{-1.23} \tag{23}$$

Using the same experimental technique, Ong and Thome [19] investigated flow patterns of R134a, R245fa and R236fa in channels with diameter 1.03, 2.2, and 3.04 mm. They proposed that macro to micro channel transition occurs at $Co \approx 0.3$–0.4. Based on that they proposed two flow pattern transition criteria for micro channels ($Co > 0.34$). Note that the confinement number for R245fa at 1.85 bar (the pressure used in obtaining the data for this study) is 0.92, which is according to [19] in the micro region. Eq. (24) gives the transition from IB to CB while Eq. (25) gives the transition from CB to A.

$$x_{IB/CB} = 0.36Co^{0.2}\left(\frac{\mu_g}{\mu_l}\right)^{0.65}\left(\frac{\rho_g}{\rho_l}\right)^{0.9}\mathrm{Re}_{go}^{0.75}Bo^{0.25}We_l^{-0.91} \tag{24}$$

$$x_{CB/A} = 0.047Co^{0.05}\left(\frac{\mu_g}{\mu_l}\right)^{0.7}\left(\frac{\rho_g}{\rho_l}\right)^{0.6}\mathrm{Re}_{go}^{0.8}We_l^{-0.91} \tag{25}$$

It can be seen from Eq. (22) that the transition from IB to CB depends on mass flux, heat flux and fluid properties while Eq. (24) adds the effect of diameter. Eqs. (23) and (25) agreed on that there is no heat flux effect on the transition from CB to A flow.

Costa-Patry et al. [47] investigated flow boiling of R134a, R1234ze(E) and R245fa in a multi microchannel copper evaporator without a transparent window for flow visualization. The local heat transfer coefficient was measured using an array of local heaters (5×7). The local heat transfer coefficient versus local vapor quality exhibited a V-shape trend for each heat flux, i.e. decreases to a minimum value then increases again. Based on that, they thought this minimum is corresponding to the transition into annular flow. Accordingly, they correlated their data as a function of operating conditions and gave Eq. (26) for the transition from CB to A. For the transition from IB to CB, they proposed using Eq. (24) of Ong and Thome [19].

$$x_{CB/A} = 425\left(\frac{\rho_g}{\rho_l}\right)^{0.1}\frac{Bo^{1.1}}{Co^{0.5}} \tag{26}$$

The above equation indicates that the vapor quality at which transition from coalescence bubble to annular flow occurs depends on heat flux, which was not the case in Eqs. (23) and (25) of Revellin-Thome and Ong-Thome. The difference is coming from the vapor quality based on which the map is developed. In the case of observing and recording the flow patterns at the exit of the evaporator, the map is based on exit quality. Once annular flow develops inside the evaporator the picture will not change at the observation section even with increasing heat flux (increasing exit quality). In the case of Costa-Patry et al., they developed their map based on local vapor quality, i.e. the vapor quality at which the local heat transfer coefficient reaches its minimum value then increases continuously with quality. Developing a transition criterion based on the trend of the heat transfer coefficient only without flow visualization may be difficult. This is because some researchers conducted flow boiling in micro tubes and found that heat transfer coefficient does not depend on vapor quality although the flow was annular.

Fig. 10 depicts the comparison of the experimental data used in this study with these three models on the mass flux versus vapor quality coordinates. It is worth mentioning that the comparison with Costa-Patry et al. is conducted at $q = 50$ kW/m^2. For the transition from IB to CB, the comparison is conducted at $q = 10$ kW/m^2. It is obvious from the figure that the model of Revellin and Thome predicts poorly the transition from CB to A flow while those of Ong and Thome and Costa-Patry et al. predict this boundary very well. If slug and churn flow reported in the present study are considered as a coalescing regime, the models of Revelling-Thome and Ong-Thome predict the boundary between IB and CB fairly well. Actually, segregating the experimental data into isolated bubbles

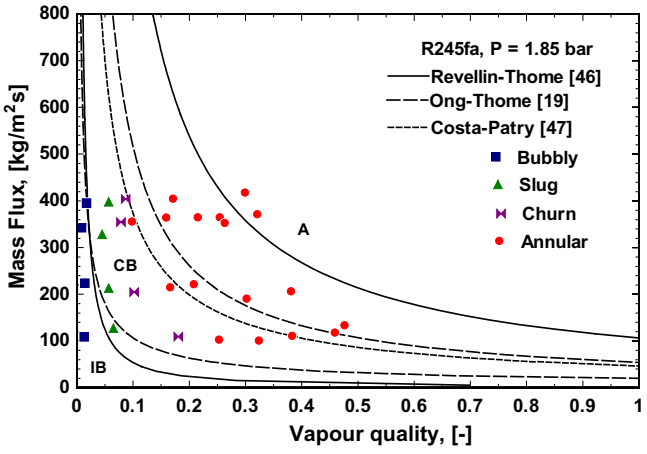

Fig. 10. Comparison of experimental data [32,33] with Revellin and Thome [46], Ong-Thome [19] and Costa-Patry [47].

and coalescing regimes is very hard without measuring the frequency. According to Revellin and Thome, isolated bubbles cover bubbly and/or slug flow. In other words, slug flow data could be located partly in the isolated bubble region and partly in the coalescing bubble region. This depends on bubble length which affects bubble velocity and consequently frequency. Increasing the heat flux shifts this boundary to the right (more slug points will be in the IB region). The sensitivity of this map to heat flux variations might make it specific and difficult to compare with other maps because it needs more information to fairly compare with, i.e. bubble frequency and coalescence rate. However, these maps are very useful for developing heat transfer mechanistic models because they incorporate the effect of heat flux.

12. Comparison with Ulmann and Brauner [48]

In this mechanistic model, Eotvos number (Eo) was used to identify the applicability range of the model. In their paper, the authors developed equations for a wide range of applications. The equations presented herein are only for minichannels applications (Eo < 0.2). The Eo value in the study of [32,33] is 0.15 based on the properties of R245fa at 1.85 bar. The transition from bubbly to slug flow was assumed to occur at a critical void fraction calculated from a train of contacting spherical bubbles with diameter equal to half tube diameter. Based on the premise that slip velocity can be ignored in microchannels, the bubbly-slug transition criterion was given as:

$$u_{ls} = \frac{1-\alpha_c}{\alpha_c} u_{gs} \tag{27}$$

The critical void fraction in the above equation was taken as 0.15 although it would be 0.166 if it was calculated based on the above assumptions given by [48]. The transition to dispersed flow was attributed to bubble breakup and transition was assumed to occur if the bubble maximum diameter is smaller than a critical value $d_{\max} \leqslant d_{cr}$. The critical value was taken as 0.5D for minichannels applications and the maximum bubble diameter was given by Eqs. (28)–(30). Eq. (29) is valid for dilute dispersions (very low gas flow rate) while Eq. (30) is valid for dense dispersions (high gas flow rates):

$$d_{\max} = Max\left((d_{\max})_0, (d_{\max})_\alpha\right) \tag{28}$$

$$(d_{\max})_0 = 30 We_{ls}^{-1} \mathrm{Re}_{ls}^{0.2} \leqslant 0.5 \tag{29}$$

$$(d_{\max})_\alpha = 174 We_{ls}^{-1} \mathrm{Re}_{ls}^{0.2} \frac{\alpha}{1-\alpha} \leqslant 0.5 \tag{30}$$

Transition from slug to aerated slug (churn flow) was assumed to occur either due to bubble breakage in the liquid slug because of turbulence or due to the wake effect behind the Taylor bubble. Both mechanisms were investigated and two transition criteria were proposed by [48] with insignificant differences. Hence, one of these mechanisms can be used. Eq. (31) below was used for this boundary in the present comparison.

$$u_{gs} + u_{ls} = 9.72 \frac{\sigma^{0.55}}{\rho_l^{0.44} \mu_l^{0.11} D^{0.44}} \tag{31}$$

Different mechanisms for the formation of annular flow were proposed and assessed by [48] using the experimental data of Triplett et al. [49] for air–water flow in micro tubes. The drop entrainment mechanism was found to give good prediction compared to the other tested mechanisms and the final criterion was given by Eq. (32).

$$U_g - U_l = 4.9 \left[1 + 1.875 \left(\frac{\mu_l^2}{\rho_l D \sigma}\right)^{0.8}\right]^{0.5} \sqrt{\frac{\sigma}{\rho_g D}} \tag{32}$$

Fig. 11 depicts the comparison of the experimental data used in this study with these transition models. The figure shows that slug and churn flow were predicted very well while bubbly and annular flows were poorly predicted. The model predicts bubby flow to occur at lower gas superficial velocity compared to the experiment while it predicts annular flow to occur at higher gas superficial velocity. Rahim et al. [50] used the data of Revellin and Thome [9] to assess this model and reported similar performance. They recommended modifying the critical void fraction value to be 0.67 rather than 0.15. On doing so, the transition boundary shifts to lower liquid superficial velocity and matched the experimental data, see the dashed line in Fig. 11.

13. Comparison with Harirchian and Garimella [51]

This map was developed based on investigating flow boiling of FC-77 in a wide range of microchannels with different cross section area. Flow patterns were classified as bubbly, slug, churn, wispy-annular and annular flow. However, they found that these flow patterns can be re-grouped into two groups namely confined and unconfined. It was found that there is a threshold cross section area below which confinement effects dominate for a fixed mass flux. It is worth mentioning here that confinement includes confined bubble, slug and annular flow. In other words, the flow pattern is considered confined when the gas phase occupies the entire channel cross section with a uniform liquid film. The confinement criterion was given by Eq. (33) using a new dimensionless number called convective-confinement number $Bd^{0.5} \times \mathrm{Re}_{lo}$.

$$Bd^{0.5} \times \mathrm{Re}_{lo} = 160 \tag{33}$$

They plotted all data on a map using the convective-confinement number for the abscissa and a dimensionless heat flux ($Bo \times \mathrm{Re}_{lo}$) for the ordinate. This map is shown in Fig. 12 compared to the experimental data used in this study. The vertical line separating confined and un-confined flow is defined by Eq. (33). The other transition line was given by Eq. (34) below. It is obvious that this map predicts poorly the experimental data. The model predicts only bubbly flow very well, where the points are located in the correct area. For this model to predict the current data the inclined line should be shifted down and the vertical line should be moved to the right.

$$Bo \times \mathrm{Re}_{lo} = 0.017 \left(Bd^{0.5} \times \mathrm{Re}_{lo}\right)^{0.7} \tag{34}$$

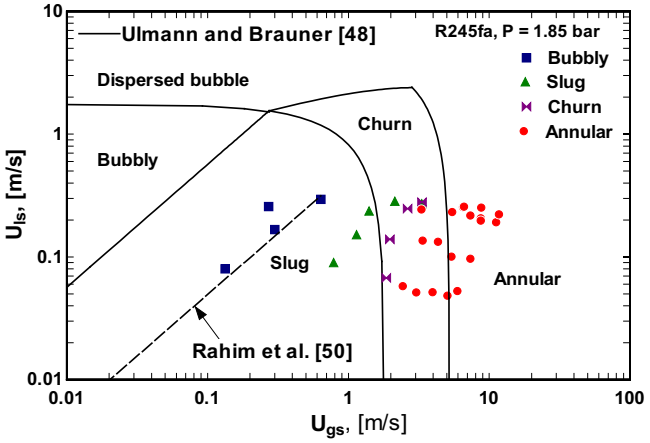

Fig. 11. Comparison of experimental data [32,33] with Ulmann and Brauner [48].

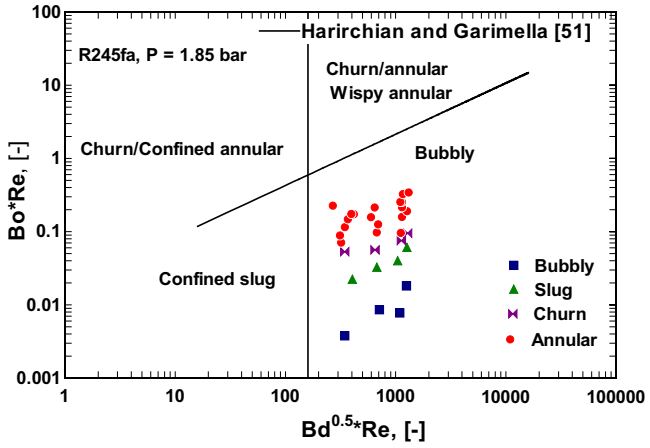

Fig. 12. Comparison of experimental data [32,33] with Harirchian and Garimella [51].

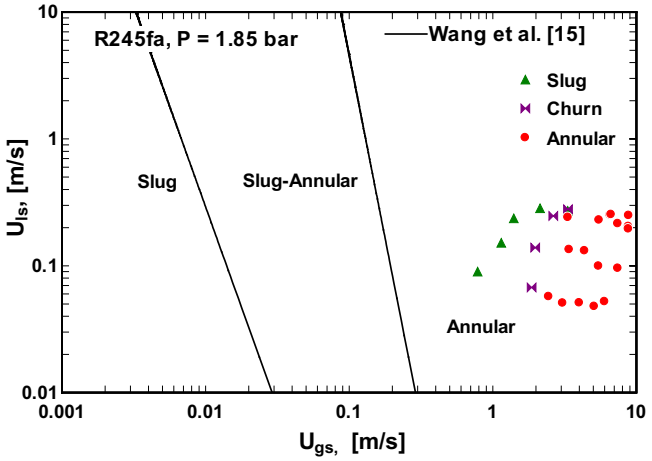

Fig. 14. Comparison of experimental data [32,33] with Wang et al. [15].

14. Comparison with Sur and Liu [52]

The experimental data used in the present study are compared with the experimental results of Sur and Liu [52] for adiabatic flow in micro tubes with diameter ranging from 0.1 to 0.324 mm, see Fig. 13. They identified four flow patterns namely bubbly, slug, ring and annular flow. It is obvious that there is a good agreement on bubbly and slug flow while poor agreement on churn and annular flow. Annular flow occurred at higher gas superficial velocity compared to the present study. However, the slopes of the transition lines are similar to that of the present experiment. It is interesting to note that although the above models failed to predict the transition boundary between bubbly and slug flow, there is a good agreement between the two experimental studies.

15. Comparison with Wang et al. [15]

As previously mentioned in the introduction section, surface wettability might affect flow pattern transition. So, it is interesting to compare the experimental data used in the present study with transition criteria that consider the effect of contact angle. Wang et al. [15] investigated the effect of surface wettability and fluid properties on gas–liquid flow in microchannels with 0.1×0.2 mm cross section. Three fluids were tested including air–water, air-kerosene and nitrogen-ethanol. The identified flow patterns were slug, slug annular, annular and parallel stratified flow. They plotted their maps using the capillary number Ca for the abscissa and Re_{gs}/Re_{ls} for the ordinate. Based on that, they proposed transition criteria including the effect of contact angle θ. The effect of contact angle was investigated using tubes made of glass ($\theta = 37^{\circ}$), modified surface glass ($\theta = 83^{\circ}$) and polydiemethylesiloxane ($\theta = 135^{\circ}$). The transition from slug to slug-annular was given by Eq. (35) while Eq. (36) gives the transition into annular.

$$Ca = 4 \times 10^{-4} \left(\frac{\pi\theta}{180}\right) \left(\frac{Re_{gs}}{Re_{ls}}\right)^{-0.76} \quad (35)$$

$$Ca = 8.6 \times 10^{-4} \left(\frac{\pi\theta}{180}\right) \left(\frac{Re_{gs}}{Re_{ls}}\right)^{-1.21} \quad (36)$$

The experimental data were compared with the above criteria on the superficial velocity coordinates, see Fig. 14. There is a doubt on the contact angle for R245fa/copper surface and therefore the present authors assumed that the contact angle for this combination is 35°, which is common for refrigerants. The comparison demonstrates that there is a poor prediction for the present experimental data. Also, the trend is completely different compared to the experimental trend. Increasing the contact angle shifts these transition lines to the right with the same slope. The performance of these prediction criteria does not change too much even when the contact angle was assumed to vary from 20° and 60°. This map predicts that gas superficial velocity at transition decreases as liquid superficial velocity increases. This trend is similar to that reported by Galvis and Culham [53] for flow boiling of water in a single rectangular channel of 0.198×0.241 mm cross section. This might open the question about the effect of channel geometry, i.e. rectangular versus circular.

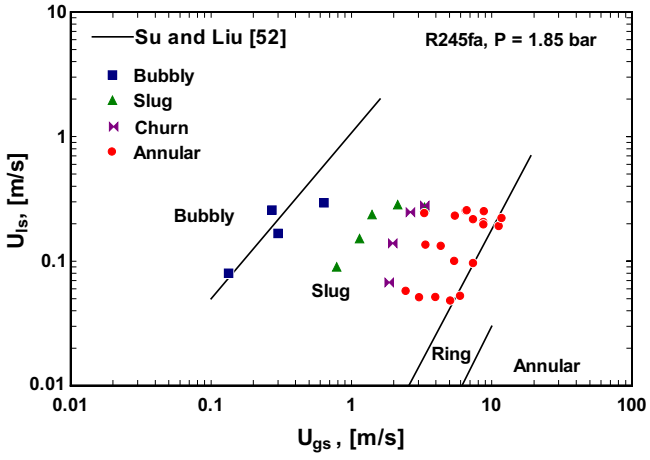

Fig. 13. Comparison of experimental data [32,33] with Sur and Liu [52].

16. Proposed Prediction Method

Figs. 15 and 16 depict a comparison between the different models for bubbly to slug and slug to annular transition respectively as examples. It is obvious from the two figures that there is a large discrepancy among all proposed models. The modified version of Ulmann and Brauner [48] model proposed by Rahim et al. [50] for bubbly-slug boundary and the model of Chen [33,41] for transition to annular flow predict the data very well.

Based on the comparison above, the present authors recommend the transition criteria given by Chen [33,41] for the slug-churn (Eqs. (9) and (10)) and churn-annular transitions (Eqs. (11)–(13)). The proposed modification by Rahim et al. [50]

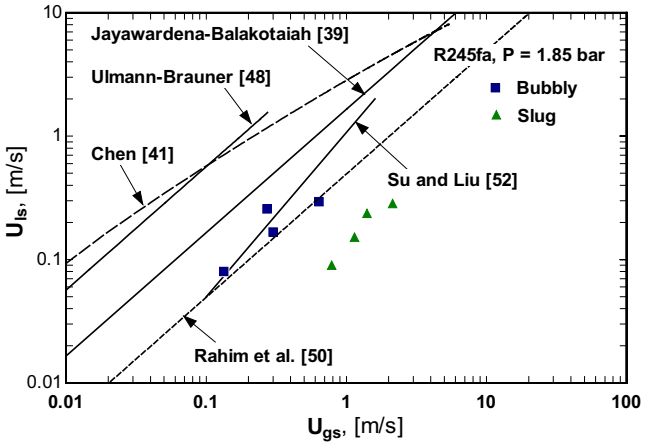

Fig. 15. comparison between different transition models for transition from bubbly to slug flow.

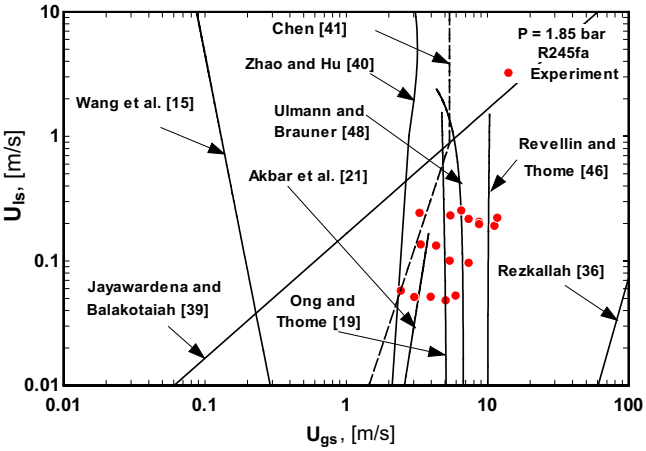

Fig. 16. Comparison between different transition models for transition from slug/churn to annular flow.

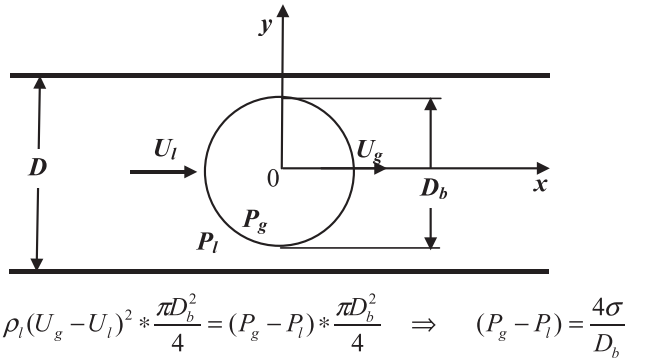

Fig. 17. Schematic drawing for the force balance on a spherical bubble with a frame of reference moving with the bubble.

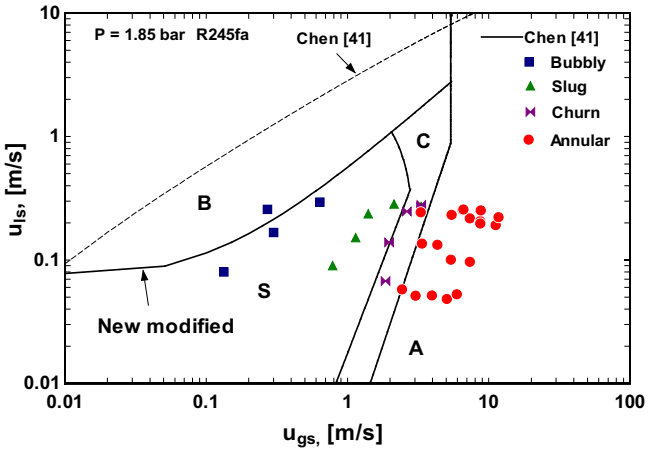

Fig. 18. Modified flow map based on that proposed by Chen [41], reported in Karayiannis et al. [33], with the new boundary proposed by the present authors (new modified).

for bubbly-slug transition could also be used. However, by inspecting Fig. 11, this modification predicts bubbly flow to occur at extremely low liquid superficial velocities. This could be due to the fact that the transition from bubbly to slug flow was assumed to occur at a fixed value of void fraction (0.67). This value is obtained when the bubble diameter at transition was assumed equal to tube diameter (confined bubble). Principally, bubble size depends on flow inertia. At very low liquid velocities, surface tension force dominates and the bubble diameter becomes large. Thus, in micro tubes at very low liquid flow rates, bubbly flow may not exist due to the confinement of the bubble and consequently slug flow develops at low liquid velocities. Another point worth mentioning is that, according to the data used in the present study [32,33] and the study of Sur and Liu [52], the calculated homogeneous void fraction ($u_{gs}/(u_{ls}+u_{gs})$) at transition is not constant. In the study of [32,33] it decreased from 0.61 at the lowest mass flux to 0.52 at the highest mass flux while in the study of Sur and Liu [52] it decreased from 0.67 to 0.56. However, it is very difficult to verify this point experimentally in microchannels due to the difficulty of measuring the void fraction. Additionally, more experimental data covering wide ranges of experimental parameters are required to verify this point even based on the calculated homogeneous void fraction. Some researchers [54,55] reported that the void fraction at the transition from bubbly to slug flow depends strongly on the initial bubble size in the mixing region. They measured the void fraction in air–water two phase flow in tubes with diameter 25 mm [54] and 28.9 mm [55]. The critical void fraction was found to decrease with increasing the initial bubble size [55]. The initial bubble diameter may be taken as the bubble departure diameter in boiling studies. However, due to thermal effects and bubble growth, the bubbly-slug transition mechanism in flow boiling in microchannels may differ from that occurring in adiabatic gas–liquid flow in large diameter channels.

Based on that, a new transition criterion from bubbly to slug flow is proposed here to take into account the effect of flow inertia, fluid properties and channel size which are thought to affect bubble confinement. Starting with a force balance on a spherical bubble with a moving frame of reference and ignoring gravity, buoyancy and viscous forces the following equation can be obtained, see schematic drawing in Fig. 17:

$$U_r^2 = \frac{4\sigma}{\rho_l D_b} \tag{37}$$

The above equation can also be written in a dimensionless form as:

$$We_r = \frac{\rho_l U_r^2 D_b}{\sigma} = 4 \tag{38}$$

According to the above equation, transition occurs when the Weber number, based on the relative velocity and bubble diameter, equals a fixed value. At transition, the bubble diameter is assumed to be the same as the tube diameter D. At this condition,

Table 2
The proposed criteria for flow patterns prediction.

Transition boundary	Equations	Author
Bubbly to slug	$We_r = \frac{\rho_l U_r^2 D}{\sigma} = 4$ $U_r = \frac{u_{gs}}{\alpha_c} - \frac{u_{ls}}{1-\alpha_c}, \quad \alpha_c = 0.67$	Present authors
Slug to churn[a]	$u_h = 2.75\sqrt{\frac{\sigma}{f_l \rho_l D}}$ $u_{gs} = 587.1\left(\frac{\mu_l}{\rho_g D}\right)^{1.447}\left(\frac{\rho_g D}{\sigma}\right)^{0.937}$ $\mathrm{Re}_{ls} = 81.08 We_{gs}^{1.626} Fr_{gs}^{*\,-0.267}$	Chen [33,41]
Churn to annular	$Fr_{gs}\,\mathrm{Re}_{gs} = 3.119\times10^{5}$ $We_{ls} = 1.567\times10^{-17}\left(Fr_{gs}\,\mathrm{Re}_{gs}\right)^{3.41}$	

$Fr_{gs} = u_{gs}/\sqrt{gD}, \quad \mathrm{Re}_{gs} = \rho_g u_{gs} D/\mu_g, \quad \mathrm{Re}_{ls} = \rho_g u_{ls} D/\mu_l, \quad We_{ls} = \rho_l u_{ls}^2 D/\sigma$
$We_{gs} = \rho_g u_{gs}^2 D/\sigma, \quad Fr_{gs}^* = u_{gs}\sqrt{\rho_g/\Delta\rho g D}, \quad u_h = u_{gs} + u_{ls}, \quad f_l = 0.046\mathrm{Re}_h^{-0.2}$
$\mathrm{Re}_h = \rho_l u_h D/\mu_l, \quad u_{gs} = xG/\rho_g, \quad u_{ls} = (1-x)G/\rho_l$

[a] This boundary needs further investigations at high liquid superficial velocities.

the critical void fraction will be 0.67 which is the same as Rahim et al. However, it is important to note that Rahim et al. [50] used the model of Ulmann and Brauner [48] which does not include the relative velocity between the phases as discussed previously, see Eq. (27). Additionally, they did not take into account the effect of tube diameter and fluid properties. The relative velocity in Eq. (38) is defined as:

$$U_r = U_g - U_l = \frac{u_{gs}}{\alpha_c} - \frac{u_{ls}}{1-\alpha_c} \tag{39}$$

In the above equation, the critical void fraction is 0.67. Fig. 18 compares the new proposed criterion against the experimental data. As seen in the figure, the new model predicts this transition boundary very well. It is interesting to note that comparing the new model to that of Chen [41] (the dashed line in Fig. 18), the two models tend to merge at the lowest gas superficial velocities. In other words, the new model agrees with Chen in that it predicts bubbly flow to occur after a certain liquid superficial velocity, i.e. when there is enough inertia force to create bubbles smaller than the tube diameter. This does not occur with the modified model of Rahim et al. [50]. To confirm this point, the bubble diameter is calculated using Eq. (37) at u_{gs} = 0.02 m/s and u_{ls} = 0.05 m/s using the properties of R245fa at 1.85 bar and the value is 2.8 mm, which is much greater than the tube diameter (1.1 mm). This bubble size gives a confined bubble which is slightly longer than the tube diameter (slug flow). According to Rahim et al. [50] at these velocities, the flow should be bubbly flow (bubbles smaller than the tube diameter).

The final equations proposed by the present authors are summarized in Table 2. As previously mentioned, dispersed bubble flow was not observed in the experimental data used in this study for the examined range of mass flux. Thus this boundary was not assessed in this study. Accordingly, Table 2 summarizes three transition boundaries namely: bubbly-slug, slug-churn and churn-annular. Some boundaries are described by more than one equation and the applicability limits of each equation depend on fluid properties and operating conditions. Therefore, a schematic drawing for these transition boundaries is included in the table for the sake of clarifying the applicability limits of each equation.

17. Conclusions

A detailed comparison of past models and correlations of flow patterns transition boundaries in micro tubes is carried out in this study. Experimental data for flow patterns recorded in a 1.1 mm diameter vertical tube made of copper at an inlet pressure of 1.85 bar, mass flux ranging from 100 to 400 kg/m^2 s and heat flux in the range of 3–25 kW/m^2 [32,33] were used. The main findings of the present study can be summarized as follows:

1. The comparison with prediction models demonstrated that there is no one map that can predict all transition boundaries with a reasonable accuracy. Annular flow occurred at lower superficial gas velocities and vapor qualities than predicted by most models.
2. The flow patterns were reported in [32,33] to vary for increasing and decreasing heat fluxes. For increasing heat flux, some occurrence of slug and churn flow was reported but a dominance of annular flow. For decreasing heat flux, bubbly, confined bubble, slug, churn and annular flow were observed. In this study, flow patterns in decreasing heat flux were used.
3. There are large discrepancies between existing prediction models although they were proposed for micro scale applications. This means that the most important parameters and mechanisms are not fully understood.
4. Among the assessed models and correlations, the flow pattern map of Chen [33,41] with the new modification developed by the present authors and given by Eqs. (37)–(39) predicted all transition boundaries very well. Thus, this map is recommended by the present authors for mini to micro scale applications.
5. However, further research is still needed and recommended to evaluate and validate the proposed map particularly at high mass fluxes, including some of the empirical constants used, for different operating ranges, fluids and passage geometries.
6. The discrepancies in the recorded flow patterns for this particular fluid and increasing and decreasing heat flux were reported in [32] and researchers must consider it when assessing their results for some of the fluids used in their experiments.

Acknowledgements

The support and comments of Drs. L. Chen, E.A. Pike-Wilson and Y. Tian are gratefully appreciated. The data used in this paper were obtained by Dr. E.A. Pike-Wilson [32,33].

References

[1] M.M. Mahmoud, T.G. Karayiannis, D.B.R. Kenning, in: Emerging Topics in Heat Transfer Enhancement and Heat Exchangers, WIT Press, 2014, pp. 321–396 (Chapter 10).
[2] I. Hassan, M. Vaillancourt, K. Pehlivan, Two-phase flow regime transitions in microchannels: a comparative experimental study, Microscale Thermophys. Eng. 9 (2) (2005) 165–182.
[3] N. Shao, A. Gavriilidis, P. Angeli, Flow regimes for adiabatic gas–liquid flow in microchannels, Chem. Eng. Sci. 64 (2009) 2749–2761.
[4] J.W. Coleman, S. Garimella, Characterization of two-phase flow patterns in small diameter round and rectangular tubes, Int. J. Heat Mass Transf. 42 (1999) 2869–2881.
[5] T.S. Zhao, Q.C. Bi, Co-current air–water two-phase flow patterns in vertical triangular microchannels, Int. J. Multiph. Flow 27 (2001) 765–782.
[6] L. Chen, Y.S. Tian, T.G. Karayiannis, The effect of tube diameter on vertical two-phase flow regimes in small tubes, Int. J. Heat Mass Transf. 49 (21–22) (2006) 4220–4230.
[7] T. Zhang, B. Cao, Y. Fan, Y. Gonthier, L. Luo, S. Wang, Gas–liquid flow in circular microchannel, Part 1: Influence of liquid physical properties and channel diameter on flow patterns, Chem. Eng. Sci. 66 (2011) 5791–5803.
[8] P.M.-Y. Chung, M. Kawaji, The effect of channel diameter on adiabatic two-phase flow characteristics in microchannels, Int. J. Multiph. Flow 30 (2004) 735–761.
[9] R. Revellin, J.R. Thome, Experimental investigation of R134a and R245fa two-phase flow in microchannels for different flow conditions, Int. J. Heat Fluid Flow 28 (1) (2007) 63–71.
[10] A.M. Barajas, R.L. Panton, The effects of contact angle on two-phase flow in capillary tubes, Int. J. Multiph. Flow 19 (2) (1993) 337–346.
[11] T. Takamasa, T. Hazuku, T. Hibiki, Experimental study of gas–liquid two phase flow affected by wall surface wettability, Int. J. Heat Fluid Flow 29 (2008) 1593–1602.
[12] C.Y. Lee, S.Y. Lee, Influence of surface wettability on transition of two-phase flow pattern in round mini-channels, Int. J. Multiph. Flow 34 (2008) 706–711.
[13] D. Huh, C.-H. Kuo, J.B. Grotberg, S. Takayama, Gas–liquid two-phase flow patterns in rectangular polymeric microchannels: effect of surface wettability, New J. Phys. 11 (2009) 75034.
[14] C. Choi, D.I. Yu, M. Kim, Surface wettability effect on flow pattern and pressure drop in adiabatic two-phase flows in rectangular microchannels with T-Junction mixer, Exp. Thermal Fluid Sci. 35 (2011) 1086–1096.
[15] X. Wang, Y. Yong, P. Fan, G. Yu, C. Yang, Z.-S. Mao, Flow regime transition for concurrent gas–liquid flow in micro-channels, Chem. Eng. Sci. 69 (2012) 578–586.
[16] C.Y. Yang, C.C. Shieh, Flow pattern of air–water and two-phase R134a in small circular tubes, Int. J. Multiph. Flow 27 (2001) 1163–1177.
[17] C. Martin-Callizo, B. Palm, W. Owhaib, R. Ali, Flow boiling visualization of R134a in a vertical channel of small diameter, J. Heat Transfer 132 (3) (2010) 1–8.
[18] A.A. Arcanjo, C.B. Tibirica, G. Ribatski, Evaluation of flow patterns and elongated bubble characteristics during the flow boiling of halocarbon refrigerants in a micro-scale channel, Exp. Thermal Fluid Sci. 34 (2010) 766–775.
[19] C.L. Ong, J.R. Thome, Macro-to-microchannel transition in two-phase flow: Part 1 – Two phase flow patterns and film thickness measurements, Exp. Thermal Fluid Sci. 35 (2011) 37–47.
[20] K. Mishima, T. Hibiki, Some characteristics of air–water two-phase flow in small diameter vertical tubes, Int. J. Multiph. Flow 22 (1996) 703–712.
[21] M.K. Akbar, D.A. Plummer, S.M. Ghiaasiaan, On gas–liquid two-phase flow regimes in microchannels, Int. J. Multiph. Flow 29 (2003) 855–865.
[22] T.G. Karayiannis, M.M. Mahmoud, D.B.R. Kenning, A study of discrepancies in flow boiling results in small to microdiameter metallic tubes, Exp. Thermal Fluid Sci. 36 (2012) 126–142.
[23] L. Consolini, J.R. Thome, Micro-channel flow boiling heat transfer of R134a, R236fa and R245fa, Microfluid. Nanofluid. 6 (2009) 731–746.
[24] M.M. Mahmoud, T.G. Karayiannis, D.B.R. Kenning, Surface effects in flow boiling of R134a in microtubes, Int. J. Heat Mass Transf. 54 (2011) 3334–3346.
[25] J.W. Coleman, S. Garimella, Two-phase flow regimes in round, square, and rectangular tubes during condensation of refrigerant R134a, Int. J. Refrig 26 (2003) 117–128.
[26] J.R. Thome, A. Bar-Cohen, R. Revellin, I. Zun, Unified mechanistic multiscale mapping of two-phase flow patterns in microchannels, Exp. Thermal Fluid Sci. 44 (2013) 1–72.
[27] C. Baldassari, M. Marengo, Flow boiling in microchannels and microgravity, Prog. Energy Combust. Sci. 39 (1) (2013) 1–36.
[28] K.J. Kubiak, M.C.T. Wilson, T.G. Mathia, Ph. Carval, Wettability versus roughness of engineering surfaces, Wear 271 (2011) 523–528.
[29] M. Kawaji, K. Mori, D. Bolintineanu, The effects of inlet geometry and gas–liquid mixing on two-phase flow in microchannels, J. Fluids Eng. 131 (2009) 41302-1–041302-7. April.
[30] H. Ide, R. Kimura, M. Kawaji, Effect of inlet geometry on adiabatic gas–liquid two-phase flow in a microchannel, Heat Transfer Eng. 30 (1–2) (2009) 37–42.
[31] J. Gregorc, I. Zun, Inlet conditions effect on bubble to slug flow transition in mini-channels, Chem. Eng. Sci. 102 (2013) 106–120.
[32] E.A. Pike-Wilson, Flow Boiling of R245fa in Vertical Small Metallic Tubes, PhD thesis, Brunel University London, UK.
[33] T.G. Karayiannis, E.A. Pike-Wilson, L. Chen, M. Mahmoud, Y. Tian, Flow Patterns and Comparison with Correlations for Vertical Flow Boiling of R245fa in Small to Micro Tubes, in: 4th Micro and Nano Flows Conference UCL, London, UK, 7–10 September, 2014.
[34] X. Huo, L. Chen, Y.S. Tian, T.G. Karayiannis, Flow boiling and flow regimes in small diameter tubes, Appl. Therm. Eng. 24 (2004) 1225–1239.
[35] E.A. Pike-Wilson, T.G. Karayiannis, Flow boiling of R245fa in 1.1 mm diameter stainless steel, brass and copper tubes, Exp. Thermal Fluid Sci. 59 (2014) 166–183.
[36] K.S. Rezkallah, Weber number based flow pattern maps for liquid–gas flows at microgravity, Int. J. Multiph. Flow 22 (6) (1996) 1265–1270.
[37] K.S. Rezkallah, Recent progress in the studies of two-phase flow at microgravity conditions, J. Adv. Space Res. 16 (1995) 123–132.
[38] L. Zhao, K.S. Rezkallah, Gas–liquid flow patterns at microgravity, Int. J. Multiph. Flow 19 (1993) 751–763.
[39] S.S. Jayawardena, V. Balakotaiah, Flow pattern transition maps for microgravity two-phase flows, AIChE J. 43 (6) (1997) 1637–1640.
[40] J.F. Zhao, W.R. Hu, Slug to annular flow transition of microgravity two-phase flow, Int. J. Multiph. Flow 26 (2000) 1295–1304.
[41] L. Chen, Flow Patterns in Upward Two-phase Flow in Small Diameter Tubes, PhD thesis, Brunel University London, UK, 2006.
[42] S. Jayanti, G.F. Hewitt, Prediction of the slug-to-churn flow transition in vertical two phase flow, Int. J. Multiph. Flow 18 (6) (1992) 847–860.
[43] Y. Taitel, Flow Pattern Transition in Two Phase Flow, in: 9th International Heat Transfer Conference, Jerusalem, Israel, 19–24 Aug., pp. 237–254, 1990.
[44] K. Mishima, M. Ishii, Flow regime transition criteria for upward two-phase flow in vertical tubes, Int. J. Heat Mass Transfer 27 (5) (1984) 723–737.
[45] D. Barnea, O. Shoham, Y. Taitel, Flow pattern transition for vertical downward two-phase flow, Chem. Eng. Sci. 37 (1982) 741–746.
[46] R. Revellin, J.R. Thome, A new type of diabatic flow pattern map for boiling heat transfer in microchannels, J. Micromech. Microeng. 17 (4) (2007) 788–796.
[47] E. Costa-Patry, J. Olivier, J.R. Thome, Heat transfer characteristics in a copper micro-evaporator and flow pattern-based prediction method for flow boiling in microchannels, Front. Heat Mass Transfer (FHMT) 3 (2012) 1–14.
[48] A. Ulmann, N. Brauner, The prediction of flow pattern maps in minichannels, Multiph. Sci. Technol. 19 (1) (2007) 49–73.
[49] A.K. Triplett, S.M. Ghiaasiaan, S.I. Abdel-Khalik, D.L. Sadowski, Gas–liquid two-phase flow in microchannels, Part I: Two-phase flow patterns, Int. J. Multiph. Flow 25 (1999) 377–394.
[50] E. Rahim, R. Revellin, J. Thome, A. Bar-Cohen, Characterization and prediction of two-phase flow regimes in miniature tubes, Int. J. Multiph. Flow 37 (2011) 12–23.
[51] T. Harirchian, S.V. Garimella, A comprehensive flow regime map for microchannel flow boiling with quantitative transition criteria, Int. J. Heat Mass Transf. 53 (2010) 2694–2702.
[52] A. Sur, D. Liu, Adiabatic air–water two-phase flow in circular microchannels, Int. J. Therm. Sci. 53 (2012) 18–24.
[53] E. Galvis, R. Culham, Measurements and flow pattern visualizations of two phase flow boiling in single channel microevaporators, Int. J. Multiph. Flow 42 (2012) 52–61.
[54] C.H. Song, H.C. No, M.K. Chung, Investigation of bubble flow developments and its transition based on the instability of void fraction waves, Int. J. Multiph. Flow 21 (1995) 381–404.
[55] H. Cheng, J.H. Hills, B.J. Azzopardi, Effects of initial bubble size on flow pattern transition in a 28.9 mm diameter column, Int. J. Multiph. Flow 28 (2002) 1047–1062.